

Membrane-induced hydroelastic migration of a particle surfing its own wave

Bhargav Rallabandi^{1,4}, Naomi Oppenheimer^{2,4}, Matan Yah Ben Zion¹ and Howard A. Stone¹

While coupling between fluid flow and soft elastic surfaces is common in biology and engineering, an analytical description is challenging as it often involves non-linear dynamics. Here we show using theory and experiments that a small particle moving along an elastic membrane through a viscous fluid is repelled from the membrane due to hydroelastic forces. The flow field produces an elastic disturbance in the membrane leading to particle-wave coupling. We derive an analytic expression for the particle trajectory and find that the normal migration velocity of the particle is quadratic in its speed and depends on a combination of the tension and bending resistance of the membrane. Experimentally, we measure the normal displacement of spheres sedimenting under gravity along a suspended elastic membrane and find quantitative agreement with the theoretical predictions with no fitting parameters. We experimentally demonstrate that the effect is strong enough for separation and sorting of particles on the basis of both their size and density. We discuss the significance of our results for particles interacting with biological membranes, and propose the use of our model for membrane elasticity measurements.

ydrodynamics at low Reynolds number prohibits a net normal force on a spherical particle moving along a rigid wall. Repulsion or attraction of the particle violates time-reversal symmetry. Relaxing the rigidity constraint breaks this symmetry; a rigid sphere moving along a soft wall (or a soft sphere along a rigid wall¹) experiences a repulsive force. Such forces have been shown to reduce drag near compressed and sheared elastic substrates²-7. Here we show that, for a thin membrane of the same material, the effect can be orders of magnitude greater, leading to sizable displacement of suspended particles.

Interactions between cell membranes and surfaces are common in many physiological and cellular processes, including blood flow in capillaries^{8–10}, filtration in the spleen^{11,12}, endocytosis¹³ and microswimming near interfaces^{14–19}. Understanding these hydroelastic interactions on the nano- and microscales is important for efficient drug delivery and release, as they significantly modify the hydrodynamic mobilities of particles such as proteins^{20–22}. Recent work has quantified many aspects of particle hydrodynamics near membranes^{23–26}, but has not addressed non-linear interactions producing repulsive forces.

We develop experiments and theory to demonstrate that a suspended particle translating tangent to a thin elastic membrane (velocity V_{\parallel}) through a viscous fluid experiences a significant migration away from the surface (velocity V_{\perp}) as a result of fluid-mediated deformations of the membrane. Our experiments comprise spherical particles sedimenting due to gravity near thin elastic sheets suspended under their own weight in silicone oil (details in Methods and Supplementary Information). Figure 1a shows snapshots, at different times, of the trajectory of a sphere near the surface of the sheet (Supplementary Movie online²⁷). The sedimentation of the sphere is accompanied by a travelling-wave deformation of the membrane and a migration of the particle away from it, resembling a particle surfing its own wave²⁸. As we show, this repulsive migration is a direct consequence of the elasticity of the membrane.

The normal motion is sensitive to the particle size and is strong enough for particle separation and sorting. Figure 2a shows a stro-

boscopic image of three different-sized particles sedimenting along the elastic sheet. The particles accelerate in the direction of gravity as a consequence of their increasing distance from the sheet over time (resulting in decreasing drag), which appears as an increasing separation distance between consecutive frames. Once settled, the particles are separated and sorted by their size (Fig. 2b): larger and denser particles experience stronger repulsion, settling further from the sheet. These results suggest the possibility of designing size-sorting devices by incorporating flexible structures in fluidic systems.

We develop a theory for the repulsive velocity V_{\perp} of the particle, accounting for hydrodynamic interactions that lead to a small but finite deformation of the elastic membrane. The membrane has a thickness b and bending rigidity B, and is held taut under a tension (force per length) T, which together keep it planar in its undeformed state S_0 . The sphere has radius a and translates with velocity $\mathbf{V} = V_{\parallel} \mathbf{e}_y + V_{\perp} \mathbf{e}_z$ as measured in the laboratory reference frame, with a separation distance h(t) that increases with time (Fig. 1). The advective nature of the membrane deformation (Fig. 1a) makes it convenient to describe the fluid-elastic problem in a local cylindrical coordinate system (r, θ, z) whose origin is instantaneously at the point on S_0 closest to the sphere (Fig. 1d), so that S_0 is identified by z=0. The fluid flow (velocity \mathbf{v} and stress $\mathbf{\sigma}$) excited by the motion of the sphere deforms the membrane to a new position $z=\zeta(\mathbf{r},t)$, where $\mathbf{r}=(r,\theta)$ is the position vector in the plane S_0 .

We consider the limit of small deflections $|\zeta|\ll h$, small separation distances $h\ll a$, and predominantly parallel motion $(V_{||}\gg V_{\perp})$. The Reynolds number in our experiments is small $(\rho_{\rm f}|{\bf V}|a/\mu\leq 0.25,$ where $\rho_{\rm f}$ and μ are the fluid's density and viscosity, respectively), so inertial contributions to either V_{\perp} or $V_{||}$ are negligible (ref. ²⁹ and Supplementary Information). Identifying $\ell=\sqrt{2ah}$ as the length scale over which stresses decay away from the sphere and defining $R=|{\bf R}|$ with ${\bf R}={\bf r}/\ell$, the fluid pressure acting to deform the membrane is approximately $p^{(0)}=\frac{6\mu V_{||}\ell R\cos\theta}{5\mu^2(1+\mu^2)^2}$, produced by the translation

of a sphere parallel to a rigid wall at S_0^{30} . Then, the membrane defor-

¹Department of Mechanical and Aerospace Engineering, Princeton University, Princeton, NJ, USA. ²Center for Computational Biology, Flatiron Institute, Simons Foundation, New York, NY, USA. ³Center for Soft Matter Research, New York University, New York, NY, USA. ⁴These authors contributed equally: Bhargav Rallabandi, Naomi Oppenheimer. *e-mail: hastone@princeton.edu

ARTICLES NATURE PHYSICS

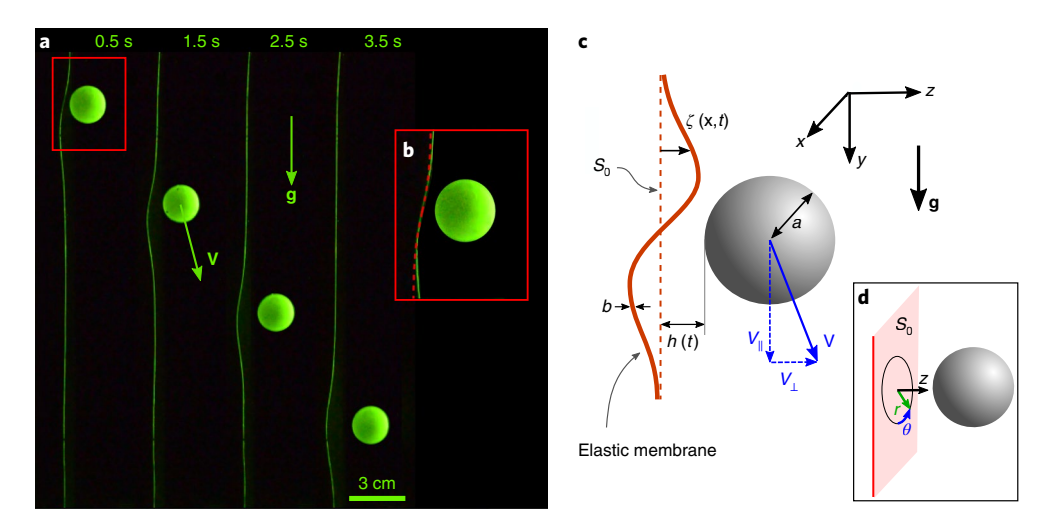


Fig. 1 | **Self-surfing and hydroelastic repulsion of a particle near a thin elastic sheet. a**, Time sequence showing experimental images of a solid sphere sedimenting under gravity near a vertically suspended rubber sheet in silicone oil. Tracking the position of the sphere at different times after release shows a spontaneous migration away from the sheet. **b**, Close-up showing the shape of the sheet and the theoretical prediction of equations (1a) and (1b) (red dashed curve) on the centre plane ($\theta = \{0, \pi\}$) with no fitting parameters; the maximum deformation amplitude is about 2 mm in both the theory and the experiments. **c**, Sketch of the system indicating the coordinate system and relevant parameters. The dashed line indicates the undeformed position S_0 (z = 0) of the elastic membrane. **d**. The local coordinate system (r, θ , z) that we use to describe the hydroelastic problem near the particle.

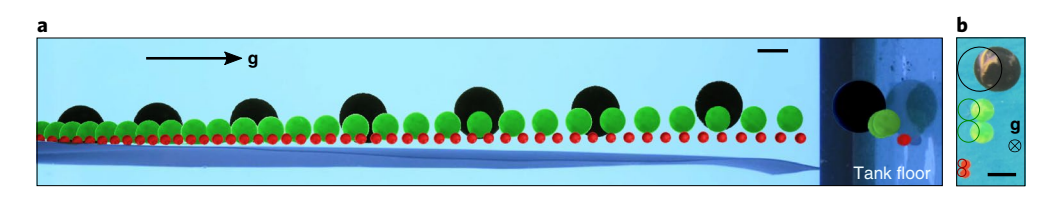


Fig. 2 | Size-dependent sorting of spherical particles sedimenting near an elastic membrane. **a**, Overlaid stroboscopic images, taken at fixed intervals of 0.33 s, indicating the motion of three different particles (all Delrin, with radii 1.5 mm (red), 4 mm (green) and 8 mm (black)). **a,b**, Final resting positions of the particles on the floor of the tank as viewed from the side (**a**) or from above (**b**), showing that the particles are sorted by their size at the end of their fall. All particles are released at the top of the tank with the same initial surface-to-surface separation distance from the sheet; initial positions are indicated as circular outlines in **b**. The scale bar is 1cm in both panels.

mation ζ is governed by the stress balance, $p^{(0)} = -(B\nabla^4 - T\nabla^2)\zeta^{31-33}$. Introducing a two-dimensional wave-vector \mathbf{k} with a polar representation (k, φ) , the deformation can be expressed in Fourier space $[\hat{f}(\mathbf{k}) = \int_{\mathbb{D}^2} f(\mathbf{R})^{-\mathbf{k}\cdot\mathbf{R}} \mathrm{d}^2\mathbf{R}$, with $\mathbf{k}\cdot\mathbf{R} = kR\cos(\varphi - \theta)$], as

$$\widehat{\zeta}(\mathbf{k}) = \frac{6\pi i \Lambda k a H}{5(k^4 + \tau H k^2)} K_0(k) \cos \varphi, \quad \text{with}$$
 (1a)

$$\Lambda = \frac{4\sqrt{2}\,\mu V_{\parallel} a^2}{BH^{1/2}}, \quad H = \frac{h}{a} \quad \text{and} \quad \tau = \frac{2Ta^2}{B}$$
 (1b)

Here, K_0 is the order-zero modified Bessel function of the second kind, $\Lambda = O(|\zeta|/h)$ is the small deformation amplitude relative to the gap height, τ is a dimensionless tension and H is the dimensionless separation distance, which varies in time. The inverse transform of equation (1a), evaluated numerically, yields the membrane shape $\zeta(\mathbf{r})$, shown in Fig. 1b with no adjustable parameters.

The deformed membrane perturbs the lubrication pressure $(p=p^{(0)}+\Lambda p^{(1)}+...)$, which results in a normal velocity of the particle V_{\perp} . We calculate V_{\perp} using the Lorentz reciprocal theorem for viscous flows³⁴, which often provides a useful tool to evaluate hydrodynamic interactions in systems with deformable boundaries^{35,36}.

In the quasi-steady limit and for small deformations (see Methods), we find

$$V_{\perp} = \frac{h}{6\pi\mu a^2 V'} \int_{S_0} (V_{||} p'(\cos\theta) \partial_r - \mu \, \partial_z \mathbf{v}' \cdot \partial_z \mathbf{v}^{(0)}) \zeta \, d^2 \mathbf{r}$$
 (2)

where $\mathbf{v}^{(0)}(\mathbf{r})$ is the fluid velocity associated with $p^{(0)}$ and primed quantities refer to the flow around a sphere translating normal to a rigid plane at S_0 .

We evaluate the integral (2) in Fourier space by applying Parseval's identity and using known results from lubrication theory (see Methods). Utilizing expression (1b) for $\hat{\zeta}(\mathbf{k})$, we obtain

$$V_{\perp} = \frac{3\mu a^2 V_{\parallel}^2}{25R} \mathcal{F}(\tau H), \quad \text{where}$$
 (3a)

$$\mathcal{F}(\tau H) = \int_0^\infty \frac{2k^4 K_0^2(k)}{k^4 + \tau H k^2} k \, dk$$
 (3b)

as our main result for the normal migration velocity of the particle. The positive-definite function $\mathcal{F}(\tau H)$ decays monotonically from

NATURE PHYSICS ARTICLES

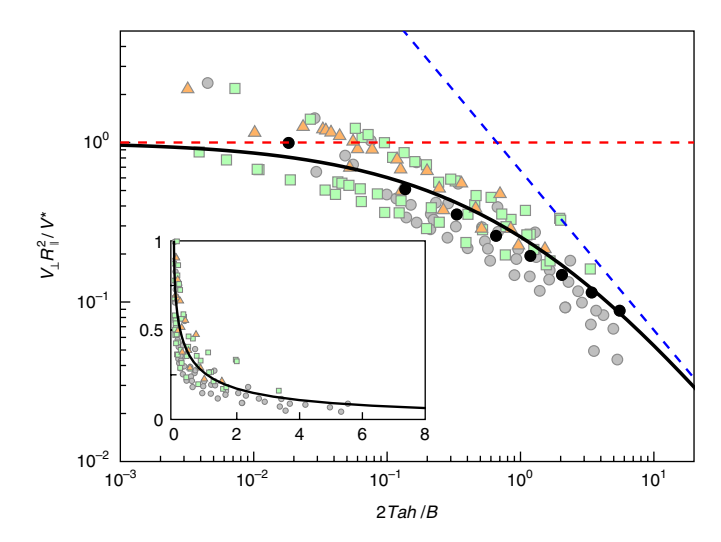


Fig. 3 | Comparison of the experimental results with the theory. Rescaled normal velocity $V_\perp \mathcal{R}_{||}^2(H)/V^*$ versus the dimensionless tension $\tau H = 2Tah/B$, showing the theoretical prediction $\mathcal{F}(\tau H)$ (equations (3a), (3b) and (4)) as a solid black curve with asymptotes indicated as dashed lines. Experimental data for several parameter combinations (circles, 0.25 mm; squares, 0.38 mm; triangles, 0.5 mm thick sheets) are in agreement with the theoretical prediction. Each set of symbols represents data for several different sphere radii and densities. Since h increases with time, each sphere samples a range of 2Tah/B values over its trajectory. The black circles indicate one such trajectory (glass sphere, a=5 mm; b=0.25 mm), where the value of 2Tah/B is initially small (due to small h; bending dominates) and decreases over the course of the motion (tension dominates). The inset shows the same data on a graph with linear axes.

unity $(\tau H \ll 1;$ bending dominates) to $\frac{2}{3\tau H}$ $(\tau H \gg 1,$ tension dominates) as shown in Fig. 3; we note that \mathcal{F} can be expressed in terms of special functions (see Methods). Thus, the sphere experiences a repulsive normal velocity V_{\perp} that is quadratic in its speed V_{\parallel} along the membrane. This quadratic dependence breaks kinematic reversibility, that is, the sphere migrates away from the sheet irrespective of the direction of its tangential motion. The repulsive migration for thin sheets is consistent with previous studies reporting lift forces near soft substrates^{3,4}, although here it is several orders of magnitude greater (for examples see Supplementary Information). The physical mechanism for the migration can be understood based on the viscous lubrication principle that fluid flow from wide openings to narrow ones creates a positive pressure and so produces $V_{\perp} > 0$ (see Supplementary Information for a detailed discussion).

In our experiments, the driving force is gravity, which is balanced by a viscous drag to establish $V_{\parallel} = 2a^2g(\Delta\rho_{\rm p})/~(9\mu\mathcal{R}_{\parallel})$, where $\Delta\rho_{\rm p} = \rho_{\rm p} - \rho_{\rm f}$. The dimensionless resistance to tangential motion, $\mathcal{R}_{\parallel}(H)$, can be approximated by its limiting form for translation along a rigid plane, provided in ref. ³⁷. Substituting the above expression for V_{\parallel} into equation (3a) yields

$$V_{\perp} = V^* \frac{\mathcal{F}(\tau H)}{\mathcal{R}_{\parallel}^2(H)}$$
 with $V^* = \frac{4a^6 g^2 (\Delta \rho_{\rm p})^2}{675 \mu B}$ (4)

Note that the relative importance of tension to bending resistance in V_{\perp} is quantified by the dimensionless parameter $\tau H = \frac{2Tah}{B}$. Since H increases with time, this ratio is not constant during the motion of a particle, so that either tension or bending may dominate during different parts of the trajectory.

The displacements y(t) and h(t) for different combinations of sphere and sheet properties are obtained from image analysis. We find

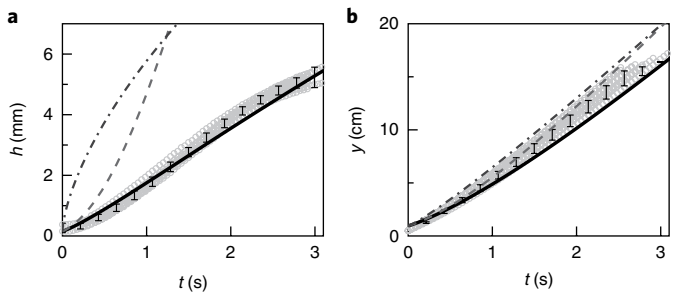


Fig. 4 | Typical trajectory of a sphere. a, Normal displacement h(t). **b**, Tangential displacement y(t). Symbols are experimental measurements (error bars indicate 1s.d.) for a 5 mm radius glass sphere and a 0.38 mm thick sheet, and the solid lines correspond to theoretical predictions accounting for bending and tension. Bending-dominated (dashed) and tension-dominated (dash-dotted) limits are indicated for comparison.

that the normal velocity V_{\perp} depends strongly on the properties of both the sheet and the sphere, and is always smaller than the sedimentation velocity V_{\parallel} (Fig. 4). Although the sheet tension decreases in the direction of gravity, we approximate it by its mean value and use $T = \frac{1}{2}(\Delta \rho_{\rm s})gLb$, where $\Delta \rho_{\rm s} = \rho_{\rm f} - \rho_{\rm s}$, to compare the experimental data with our theoretical predictions; relaxing this simplification yields only minor differences (see Supplementary Information). Thus, $\tau = \frac{gLa^2(\Delta \rho_{\rm s})}{B} = \frac{12(1-\nu^2)gL(\Delta \rho_{\rm s})}{E(b/a)^2}$ (compare equa-

tion (1b)), where $\nu \approx 0.48$ is the Poisson ratio and E is the Young's modulus of the sheet. τ is greater for thinner sheets and larger particles, and is in the range 0.25–8 in our experiments. Recalling that the relative magnitudes of tension and bending are determined by τH (see for example equation (4)), we expect bending to be important at small separation distances $\tau H \ll 1$, and for tension to dominate for larger separation distances with $\tau H \gg 1$; our experimental data span both of these limiting regimes and are in good agreement with the theoretical prediction (Fig. 3).

We compute the trajectory (y(t), h(t)) by numerically integrating the velocity components, V_{\perp} (equation (4)) and V_{\parallel} . Figure 4 shows the trajectory of a sphere with a particular combination of sheet and particle properties. The theoretical predictions for the displacement, without adjustable parameters, are plotted as solid lines, showing that both bending (dashed) and tension (dashdotted) contributions must be incorporated to achieve quantitative agreement with the experimentally measured trajectories (grey circles).

The system transitions between bending- and tension-dominated regimes as the separation distance increases over time. This transition is indicated for a single trajectory (black circles in Fig. 3), but is clearly observed when varying system parameters such as particle size and density as well as the sheet bending rigidity, as shown in Fig. 3.

Neglecting the weak (logarithmic) dependence of V_{\parallel} on H, the normal velocity is constant in the bending-dominated regime $(H\ll\tau^{-1})$, that is, the separation distance increases linearly with time, $h\approx \frac{3\mu a^2 V_{\parallel}^2}{25B}t$ for sufficiently small h. In our experiments, we do not observe trajectories that are characterized by bending alone, although bending is likely to dominate for smaller particles (since $\tau \propto a^2$). In the tension-dominated limit ($\tau H\gg 1$; long times or thin sheets), integrating equations (3a) and (3b) yields $h\approx \sqrt{2\mu at/(25T)}\ V_{\parallel}$, again neglecting the dependence of V_{\parallel} on H. For our gravity-driven experiments, this expression reduces to $h\approx h^*\sqrt{x/L}$, where $h^*=\frac{2\sqrt{2}}{15}\left(\frac{\Delta\rho_p}{\Delta\rho_s}\right)^{\frac{1}{2}}a^{\frac{3}{2}}b^{-\frac{1}{2}}$. We find a good col-

lapse of the measured trajectories for different particle sizes, as indi-

ARTICLES NATURE PHYSICS

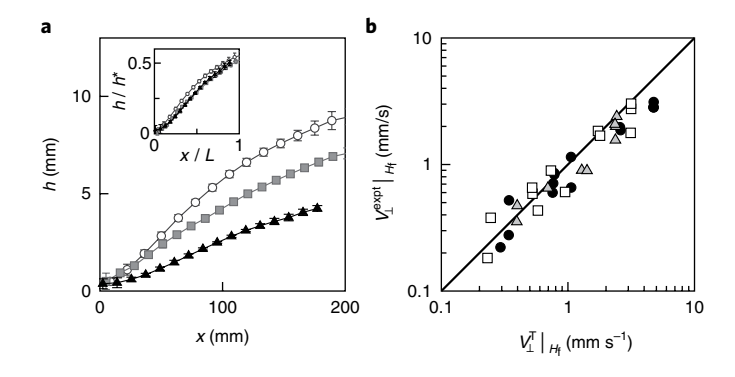


Fig. 5 | The normal migration depends on the size and the density of the particles, as well as the properties of the sheet. a, Experimental trajectories of three different spheres (circles, glass, $a_p = 5$ mm; squares, glass, $a_p = 3$ mm; triangles, Delrin, $a_p = 6$ mm) near a sheet of thickness b = 0.25 mm. Inset, rescaled trajectories for tension-dominated dynamics as discussed in the text. Error bars indicate 1s.d. **b,** By the end of their trajectories ($H = H_l$), the normal velocity is dominated by tension; measured velocities (symbols) are plotted against the tension-dominated theoretical prediction, $V_{\perp}^{\rm T}|_{H_l} = \frac{4a^4g^2(\Delta\rho_p)^2}{2,025\mu TH_l \mathcal{R}_{\parallel}^2(H_l)}$. The data span all sheet thicknesses (circles, b = 0.25 mm; squares, b = 0.38 mm; triangles,

thicknesses (circles, b = 0.25 mm; squares, b = 0.38 mm; triangles, b = 0.5 mm) and sphere properties (not indicated).

cated in Fig. 5a. For all the experiments, we can extract data points where the system is tension dominated. In particular, the measured V_{\perp} of each particle at the end of its trajectory (for which particles assume final separation distances $H = H_{\rm f}$) is well described by the

tension-dominated limit of the theory, $V_{\perp}^{\rm T}|_{H_{\rm f}} = \frac{4a^4g^2(\Delta\rho_{\rm p})^2}{2,025\mu T} \frac{1}{H_{\rm f}\mathcal{R}_{||}(H_{\rm f})}$, as shown in Fig. 5b.

We comment on extensions of the theoretical framework developed here. It is possible to include a confining potential G (a force per volume), such that the membrane deformation is governed by $p^{(0)} = -(B\nabla^4 + T\nabla^2 + G)\zeta$. Such a confining potential may be externally applied using an optical trap³⁸, or for biological membranes can arise from a non-zero curvature³³, finite system size or an underlying cytoskeleton^{23,39}. In macroscopic systems, such a potential often results from a body force, such as gravity, acting normal to the membrane. The effect of this added potential to the normal velocity V_{\perp} is accounted for by modifying the denominator of equations (3a) and (3b) to $(k^4 + \tau Hk^2 + \gamma H^2)$, where $\gamma = G\ell^4/(BH^2) = 4Ga^4/B$. For a cylindrical object translating perpendicular to its axis (here the xaxis, compare Fig. 1b), the only modification to V_{\perp} involves replacing $K_0(k)$ by $\frac{5}{3}\sqrt{\frac{2}{k}}e^{-k}$ in equations (3a) and (3b); the results of refs ^{3,4} then correspond to the limit $\gamma \gg 1$ (Methods). Finally, we note

that the mechanism for hydroelastic migration and the scaling laws obtained here persist for active particles (for example microswimmers), but with modified prefactors that depend on the details of the propulsion mechanism. In particular, a fore–aft pressure asymmetry due to the motion of active particles⁴⁰ is sufficient to induce migration (see Supplementary Information).

We have demonstrated theoretically and experimentally that a particle moving along a membrane will experience a hydroelastic repulsion. There are several consequences of this effect. (1) A swimming bacterium ($\approx 1\,\mu\text{m}$) near a membrane $B\approx 10k_{\text{B}}T$ (T denotes temperature) with a typical speed ($\approx 30\,\mu\text{m}\,\text{s}^{-1}$) can be hydroelastically repelled at a speed that is comparable to its own. (2) The repulsive migration of a microswimmer propelled near a bio-membrane is expected to be several orders of magnitude greater than the lift generated by a compressible substrate (such as the cytoskeleton, $G\approx 10$ –1000 Pa). On macroscopic scales, the particles in our experiments experience a force greater by about three orders of

magnitude than they would in a comparable experiment with a soft substrate (refs 4,5,7; Supplementary Information). (3) Our model suggests the possibility of a non-intrusive measurement of the elastic properties of biological membranes, one that does not require thermal equilibrium (for example by using a micrometre-sized bead and optical or magnetic tweezers (4),42). (4) Small thermal fluctuations of a bio-membrane result in a reduced effective bending rigidity (4) and are therefore expected to enhance the repulsive migration due to hydroelastic surfing (Supplementary Information) (though shear may suppress such fluctuations (5) Our macroscopic sedimentation experiments show that the hydroelastic repulsion is sensitive enough to the size of the particle for sorting and separation purposes. This large number of possibilities suggests new opportunities for experiments and theory that take advantage of hydroeleastic lift generated by flexible sheets.

Online content

Any methods, additional references, Nature Research reporting summaries, source data, statements of data availability and associated accession codes are available at https://doi.org/10.1038/s41567-018-0272-z.

Received: 19 March 2018; Accepted: 1 August 2018; Published online: 17 September 2018

References

- Abkarian, M., Lartigue, C. & Viallat, A. Tank treading and unbinding of deformable vesicles in shear flow: determination of the lift force. *Phys. Rev. Lett.* 88, 068103 (2002).
- Coyle, D. J. Forward roll coating with deformable rolls: a simple onedimensional elastohydrodynamic model. *Chem. Eng. Sci.* 43, 2673–2684 (1988).
- Sekimoto, K. & Leibler, L. A mechanism for shear thickening of polymerbearing surfaces: elasto-hydrodynamic coupling. *Europhys. Lett.* 23, 113 (1993).
- Skotheim, J. M. & Mahadevan, L. Soft lubrication. Phys. Rev. Lett. 92, 245509 (2004).
- Skotheim, J. M. & Mahadevan, L. Soft lubrication: the elastohydrodynamics of nonconforming and conforming contacts. *Phys. Fluids* 17, 092101 (2005).
- Snoeijer, J. H., Eggers, J. & Venner, C. H. Similarity theory of lubricated Hertzian contacts. *Phys. Fluids* 25, 101705 (2013).
- Saintyves, B., Jules, T., Salez, T. & Mahadevan, L. Self-sustained lift and low friction via soft lubrication. Proc. Natl Acad. Sci. USA 113, 5847–5849 (2016).
- 8. Secomb, T. W., Skalak, R., Özkaya, N. & Gross, J. Flow of axisymmetric red blood cells in narrow capillaries. *J. Fluid. Mech.* **163**, 405–423 (1986).
- Noguchi, H. & Gompper, G. Shape transitions of fluid vesicles and red blood cells in capillary flows. Proc. Natl Acad. Sci. USA 102, 14159–14164 (2005).
- Dzwinel, W., Boryczko, K. & A, Y. D. A discrete-particle model of blood dynamics in capillary vessels. *J. Colloid Interface. Sci.* 258, 163–173 (2003).
- Jandl, J. H., Greenberg, M., Yonemoto, R. & Castle, W. Clinical determination of the sites of red cell sequestration in hemolytic anemias. *J. Clin. Invest.* 35, 842–867 (1956).
- Pivkin, I. V. et al. Biomechanics of red blood cells in human spleen and consequences for physiology and disease. *Proc. Natl Acad. Sci. USA* 113, 7804–7809 (2016).
- Goldstein, J. L., Anderson, R. G. W. & Brown, M. S. Coated pits, coated vesicles, and receptor-mediated endocytosis. *Nature* 279, 679–685 (1979).
- Trouilloud, R., Tony, S. Y., Hosoi, A. E. & Lauga, E. Soft swimming: exploiting deformable interfaces for low Reynolds number locomotion. *Phys. Rev. Lett.* 101, 048102 (2008).
- Giacché, D., Ishikawa, T. & Yamaguchi, T. Hydrodynamic entrapment of bacteria swimming near a solid surface. Phys. Rev. E 82, 056309 (2010).
- Dias, M. A. & Powers, T. R. Swimming near deformable membranes at low Reynolds number. *Phys. Fluids* 25, 101901 (2013).
- Ledesma-Aguilar, R. & Yeomans, J. M. Enhanced motility of a microswimmer in rigid and elastic confinement. *Phys. Rev. Lett.* 111, 138101 (2013).
- Boryshpolets, S. et al. Different swimming behaviors of sterlet (Acipenser ruthenus) spermatozoa close to solid and free surfaces. Theriogenology 79, 81–86 (2013).
- Lushi, E., Wioland, H. & Goldstein, R. E. Fluid flows created by swimming bacteria drive self-organization in confined suspensions. *Proc. Natl Acad. Sci.* USA 111, 9733–9738 (2014).
- Lodish, H et al. Molecular Cell Biology 3rd edn (Scientific American Books, New York, NY, 1995).

NATURE PHYSICS ARTICLES

- Fradin, C., Abu-Arish, A., Granek, R. & Elbaum, M. Fluorescence correlation spectroscopy close to a fluctuating membrane. *Biophys. J.* 84, 2005–2020 (2003).
- Kimura, Y., Mori, T., Yamamoto, A. & Mizuno, D. Hierarchical transport of nanoparticles in a lyotropic lamellar phase. J. Phys. Condens. Matter 17, S2937 (2005).
- 23. Bickel, T. Brownian motion near a liquid-like membrane. Eur. Phys. J. E 20, 379–385 (2006).
- Bickel, T. Hindered mobility of a particle near a soft interface. *Phys. Rev. E* 75, 041403 (2007).
- 25. Daddi-Moussa-Ider, A., Lisicki, M. & Gekle, S. Mobility of an axisymmetric particle near an elastic interface. *J. Fluid. Mech.* **811**, 210–233 (2017).
- Daddi-Moussa-Ider, A. & Gekle, S. Hydrodynamic mobility of a solid particle near a spherical elastic membrane: axisymmetric motion. *Phys. Rev. E* 95, 013108 (2017).
- Rallabandi, B., Oppenheimer, N., Zion, M. Y. B. & Stone, H. A. Membrane induced hydroelastic migration of a particle surfing its own wave. *figshare* https://figshare.com/articles/All_Figure_Data/6030572/9 (2018).
- Bush, J. W. M. Pilot-wave hydrodynamics. Annu. Rev. Fluid Mech. 47, 269–292 (2015).
- Becker, L. E., McKinley, G. H. & Stone, H. A. Sedimentation of a sphere near a plane wall: weak non-Newtonian and inertial effects. *J. Non-Newtonian Fluid Mech.* 63, 201–233 (1996).
- O'Neill, M. E. & Stewartson, K. On the slow motion of a sphere parallel to a nearby plane wall. *J. Fluid. Mech.* 27, 705–724 (1967).
- Landau, L. D., & Lifshitz, E. M. Theory of Elasticity. Volume 7 of Course of Theoretical Physics (Elsevier, New York, NY, 1986).
- Helfrich, W. Elastic properties of lipid bilayers: theory and possible experiments. Z. Naturforsch. C 28, 693–703 (1973).
- Seifert, U. Configurations of fluid membranes and vesicles. Adv. Phys. 46, 13–137 (1997).
- 34. Happel, J. & Brenner, H. Low Reynolds Number Hydrodynamics with Special Application to Particulate Media (Prentice-Hall, The Hague, 1965).
- Berdan, C. II & Leal, L. G. Motion of a sphere in the presence of a deformable interface: I. Perturbation of the interface from flat: the effects on drag and torque. J. Colloid Interface Sci. 87, 62–80 (1982).
- 36. Yang, S.-M. & Leal, L. G. Motions of a fluid drop near a deformable interface. *Int. J. Multiph. Flow* 16, 597–616 (1990).
- Goldman, A. J., Cox, R. G. & Brenner, H. Slow viscous motion of a sphere parallel to a plane wall—I Motion through a quiescent fluid. *Chem. Eng. Sci.* 22, 637–651 (1967).
- Verhoeff, A. A., Lavergne, F. A., Bartolo, D., Aarts, D. G. A. L. & Dullens, R. P. A. Optical trapping of interfaces at ultra-low interfacial tension. *Soft Matter* 11, 3100–3104 (2015).
- Fournier, J.-B., Lacoste, D. & Raphaël, E. Fluctuation spectrum of fluid membranes coupled to an elastic meshwork: jump of the effective surface tension at the mesh size. *Phys. Rev. Lett.* 92, 018102 (2004).

- Spagnolie, S. E. & Lauga, E. Hydrodynamics of self-propulsion near a boundary: predictions and accuracy of far-field approximations. *J. Fluid. Mech.* 700, 105–147 (2012).
- Shlomovitz, R., Evans, A. A., Boatwright, T., Dennin, M. & Levine, A. J. Measurement of monolayer viscosity using noncontact microrheology. *Phys. Rev. Lett.* 110, 137802 (2013).
- Boatwright, T., Dennin, M., Shlomovitz, R., Evans, A. A. & Levine, A. J. Probing interfacial dynamics and mechanics using submerged particle microrheology. II. Experiment. *Phys. Fluids* 26, 071904 (2014).
- Peliti, L. & Leibler, S. Effects of thermal fluctuations on systems with small surface tension. *Phys. Rev. Lett.* 54, 1690 (1985).
- 44. Nelson, D. & Peliti, L. Fluctuations in membranes with crystalline and hexatic order. *J. Phys. (Paris)* 48, 1085–1092 (1987).
- Derks, D., Aarts, D. G. A. L., Bonn, D., Lekkerkerker, H. N. W. & Imhof, A. Suppression of thermally excited capillary waves by shear flow. *Phys. Rev. Lett.* 97, 038301 (2006).

Acknowledgements

The authors acknowledge support from the National Science Foundation via award DMS-1614907, and partial support from the Carbon Mitigation Initiative of Princeton University. M.Y.B.Z. acknowledges support by the Center for Bio Inspired Energy Sciences, an Energy Frontier Research Center funded by the DOE, Office of Sciences, Basic Energy Sciences, under award DE-SC0000989 (Paul M. Chakin). We thank T. Salez for preliminary discussions, M. Shelley for helpful ideas and J. Nunes, A. Perazzo and Y. E. Yu for their help with the experiments.

Author contributions

B.R. and N.O. contributed equally to this work. B.R., N.O. and H.A.S conceived the project and developed the theory. B.R., N.O. and M.Y.B.Z. performed the experiments. All authors analysed and interpreted the data and wrote the paper.

Competing interests

The authors declare no competing interests.

Additional information

Supplementary information is available for this paper at https://doi.org/10.1038/s41567-018-0272-z.

Reprints and permissions information is available at www.nature.com/reprints.

Correspondence and requests for materials should be addressed to H.A.S.

Publisher's note: Springer Nature remains neutral with regard to jurisdictional claims in published maps and institutional affiliations.

ARTICLES NATURE PHYSICS

Methods

Theoretical derivation. To calculate the normal velocity, equations (3a) and (3b), we use the Lorentz reciprocal theorem $\int_S \mathbf{n} \cdot \boldsymbol{\sigma} \cdot \mathbf{v}' \mathrm{d}^2 \mathbf{r} = \int_S \mathbf{n} \cdot \boldsymbol{\sigma}' \cdot \mathbf{v} \mathrm{d}^2 \mathbf{r}$, where \mathbf{v}' and $\mathbf{\sigma}'$ are the known fluid velocity and stress fields around a sphere moving perpendicular to a *rigid* wall, and \mathbf{n} is the unit normal to the surface. The integration is over the *undeformed* bounding surface of the fluid domain S, which comprises S_0 , the particle surface S_p and a surface at infinity S_∞ . With the conditions $\mathbf{v} = \mathbf{v}' = \mathbf{0}$ on S_p (no-slip), and $\mathbf{v} = -\mathbf{V}$ (and $\mathbf{v}' = -\mathbf{V}'$) on S_∞ , the reciprocal relation becomes $F_\perp' V_\perp = \int_{S_0} \mathbf{n} \cdot \mathbf{\sigma}' \cdot (\mathbf{v} + V) \, \mathrm{d}^2 \mathbf{r}$, where F_\perp' is the applied force on the sphere in the auxiliary (primed) problem ⁴⁶.

To obtain ${\bf v}$ on S_0 (z=0), we use the no-slip condition ${\bf v}|_{z=\zeta}=-{\bf V}-{\bf e}_z V_{\parallel}\partial_y\zeta$, where we have assumed a quasi-static membrane deformation in the particle reference frame ($|\partial_t\zeta|\ll V_{\parallel}||\partial_y\zeta|$). We map this boundary condition onto the plane S_0 by means of a Taylor expansion, ${\bf v}|_{S_0}\approx {\bf v}|_{z=\zeta}-\zeta\partial_z {\bf v}|_{S_0}=-{\bf V}-{\bf e}_z V_{\parallel}\partial_y\zeta-\zeta\partial_z {\bf v}|_{S_0}$. Next, we approximate the velocity gradient by that of the zeroth-order problem (translation parallel to a planar wall), $\partial_z {\bf v} \approx \partial_z {\bf v}^{(0)}$. Recognizing that the applied force on the sphere in the auxiliary problem is $F'=6\pi\mu a^2V'/h$ in the lubrication limit yields equation (2). We then use standard results from lubrication theory ${\bf v}^{(0,46)}$: $p'=-\frac{3MV'\ell'^2}{2h^3(1+R^2)^2}\partial_z {\bf v}{\bf v}'|_{z=0}=-\frac{3V'\ell R}{h^2(1+R^2)^2}{\bf e}_z$, and $\partial_z {\bf v}^{(0)}|_{z=0}=\frac{2V_{\parallel}}{5h(1+R^2)}\left\{\left(7-\frac{6}{1+R^2}\right)\cos\theta-\sin\theta\right\}$.

Evaluating the resulting definite integral in Fourier space finally results in (3a) and (3b). The result can be expressed in terms of known functions as

$$V_{\perp} = \frac{3\mu a^2 V_{\parallel}^2}{25B} \mathcal{F}(\tau H), \text{ with}$$
 (5a)

$$\mathcal{F}(\tau H) \equiv \int_0^\infty \frac{2k^4 K_0^2(k)}{k^4 + \tau H k^2} k \, dk$$
 (5b)

$$= \frac{\sqrt{\pi}}{2} Meijer G_{2,4}^{4,1} \left[\tau H \middle| \begin{array}{c} 0, \frac{3}{2} \\ 0, 1, 1, 1 \end{array} \right]. \tag{5c}$$

As noted in the main text, for $\tau H \ll 1$, that is the bending-dominated limit, equation (5b) gives $\mathcal{F}=1$. In the opposite, tension-dominated limit, $\tau H \gg 1$, equation (5b) gives $\mathcal{F}=\frac{2}{3\tau H}$.

For a cylinder translating tangent to the membrane, the normal velocity is

$$V_{\perp}^{\text{cyl}} = \frac{2\mu a^2 V_{||}^2}{3B} \mathcal{F}^{\text{cyl}}(\tau H), \text{ with}$$
 (6a)

$$\mathcal{F}^{\text{cyl}}(\tau H) = \int_0^\infty \frac{2k^4 e^{-2k}}{k^4 + \tau H k^2} dk = 1 - \sqrt{\tau H} \left[\pi \cos(2\sqrt{\tau H}) \right]$$

$$-2 \operatorname{Ci}(2\sqrt{\tau H}) \sin(2\sqrt{\tau H})$$

$$\left[+2 \operatorname{Si}(2\sqrt{\tau H}) \cos(\sqrt{\tau H}) \right]$$
(6b)

where Ci and Si are cosine and sine integrals, respectively.

Conversely, if the sphere is forced to translate parallel to the soft membrane without normal migration (by the application of an external normal force), it will experience a counterbalancing repulsive hydrodynamic force $F_{\perp}^{\rm H}=6\pi\mu V_{\perp}a^2/h$. Similarly, a cylinder forced to translate tangent to the soft membrane experiences a repulsive force per unit length

$$f_{\perp}^{\text{H,cyl}} = 3\sqrt{2}\pi\mu V_{\perp}^{\text{cyl}} \left(\frac{a}{h}\right)^{3/2} = \frac{2\sqrt{2}\pi\mu^2 a^{7/2} V_{||}^2}{Bh^{3/2}} \mathcal{F}^{\text{cyl}}(\tau H)$$
 (7)

Experimental details. Our experimental setup consists of a tank

(16 cm × 16 cm × 30 cm) containing silicone oil (density 0.97 g cm⁻³, viscosity 1 Pa s; Sigma Aldrich); see an image of the setup in Supplementary Information. Silicone rubber sheets (Marian; Shore A durometer 10) of size 8 cm × 30 cm, density $\rho_s = 1.1 \, \text{g cm}^{-3}$ and thicknesses b (0.25, 0.38, 0.5 mm) are suspended close to the middle of the container such that their top end is held fixed and their bottom end is free. The immersed length of the sheets in the oil is $L = 20 \, \text{cm}$. Being denser than the fluid, the sheets are suspended under their own weight, which provides tension T in the range 0.03–0.06 N m⁻¹.

We use a linear extension experiment to measure the Young's modulus of each sheet by suspending it in air and progressively loading (and subsequently unloading) with known weights attached to its bottom edge. We find a linear response with no measurable hysteresis up to about 9% linear strain, and extract a Young's modulus of $E\approx 245$ kPa for all the sheets independent of their thickness. The bending rigidity of the sheets is calculated as $B=\frac{Eb^3}{12(1-\nu^2)}$, using $\nu\approx 0.48$ as the Poisson ratio for silicone rubber; for the sheets used in our experiments, B is in the range of $0.4-3.3\,\mu\mathrm{N}\,\mathrm{m}$.

Spheres of different materials (Delrin, 1.4 g cm⁻³; borosilicate glass, 2.4 g cm⁻³; stainless steel, 8.05 g cm⁻³), with radii in the range 2–8 mm, are released in close proximity to the top of the sheet. The point of release is halfway across the width of the sheet (in the *x*-direction, Fig. 1) so that the spheres are symmetric with respect to either edge of the sheet. The motion of the spheres is recorded at 30 frames s⁻¹ with a camera (Nikon D5100); motion in the *x*-direction is found to be negligible. All measurements were carried out at an ambient temperature of 22+0.5 °C

Data availability

The experimental data for the plots within this paper are available from the figshare repository²⁷. The same repository contains a movie corresponding to Fig. 1a. Raw image data and other supporting data relevant to this study are available from the authors upon request.

References

46. Cox, R. G. & Brenner, H. The slow motion of a sphere through a viscous fluid towards a plane surface—II small gap widths, including inertial effects. *Chem. Eng. Sci.* **22**, 1753–1777 (1967).



SUPPLEMENTARY INFORMATION

https://doi.org/10.1038/s41567-018-0272-z

In the format provided by the authors and unedited.

Membrane-induced hydroelastic migration of a particle surfing its own wave

Bhargav Rallabandi^{1,4}, Naomi Oppenheimer^{2,4}, Matan Yah Ben Zion[®] and Howard A. Stone[®] ^{1*}

¹Department of Mechanical and Aerospace Engineering, Princeton University, Princeton, NJ, USA. ²Center for Computational Biology, Flatiron Institute, Simons Foundation, New York, NY, USA. ³Center for Soft Matter Research, New York University, New York, NY, USA. ⁴These authors contributed equally: Bhargav Rallabandi, Naomi Oppenheimer. *e-mail: hastone@princeton.edu

Supplementary Information

Membrane induced hydroelastic migration of a particle surfing its own wave

Bhargav Rallabandi,^{1,*} Naomi Oppenheimer,^{2,*} Matan Yah Ben Zion,³ and Howard A. Stone^{1,†}

¹Department of Mechanical and Aerospace Engineering, Princeton University, Princeton, New Jersey 08544, USA ²Center for Computational Biology, Flatiron Institute, Simons Foundation, New York, NY 10010, USA ³Center for Soft Matter Research, New York University, NY 10003, USA

A. Experimental setup

Our experimental setup is presented in Fig. S1. The silicone rubber sheets are held by a cylindrical rod at the top of the container and suspended in silicone oil under their own weight. Spheres are dropped close to the middle of the sheet, starting from a position close to the sheet. Videos of the spheres' motion are captured from the side and later analyzed using Matlab and Python. More of the experimental details are discussed in the Methods section of the main text.



FIG. S1. Experimental setup: silicone rubber sheets of size 8 cm \times 30 cm are suspended in silicone oil (viscosity 1 Pa·s) in a glass tank of dimensions 16 cm \times 16 cm \times 30 cm. The immersed length of the sheet is 20 cm. The sheet is suspended under gravity with its top end held on a cylindrical rod and its bottom end free.

^{*} These authors contributed equally

 $^{^{\}dagger}$ hastone@princeton.edu

B. Intuitive explanation of the migration velocity

A schematic representation of the mechanism leading to the generation of a repulsive normal force on a sphere translating next to a membrane is given in Fig. S2. The mechanism is based on the viscous lubrication principle that fluid flow from wide openings to narrow ones creates a positive pressure. The leading-order problem corresponds to the sphere translating along a rigid plane, which has an antisymmetric pressure distribution with higher pressure near the front of the sphere (the upstream end) and a lower pressure at the back (the downstream end); see Fig. S2a. This pressure distribution deforms the membrane in such a way that the width of the gap between the sphere and the membrane is greater at the front and smaller at the back (Fig. S2b). This change in geometry implies a fluid flow in a gap that is wider in the front than it is in the back, and is analogous to the flow under a slider block [1] (see Fig. S2c), although differing in details. Such a flow generates, at next order, a positive pressure in the gap and thus a repulsive hydrodynamic force. In our case, the particle is free to move and consequently migrates away from the membrane.

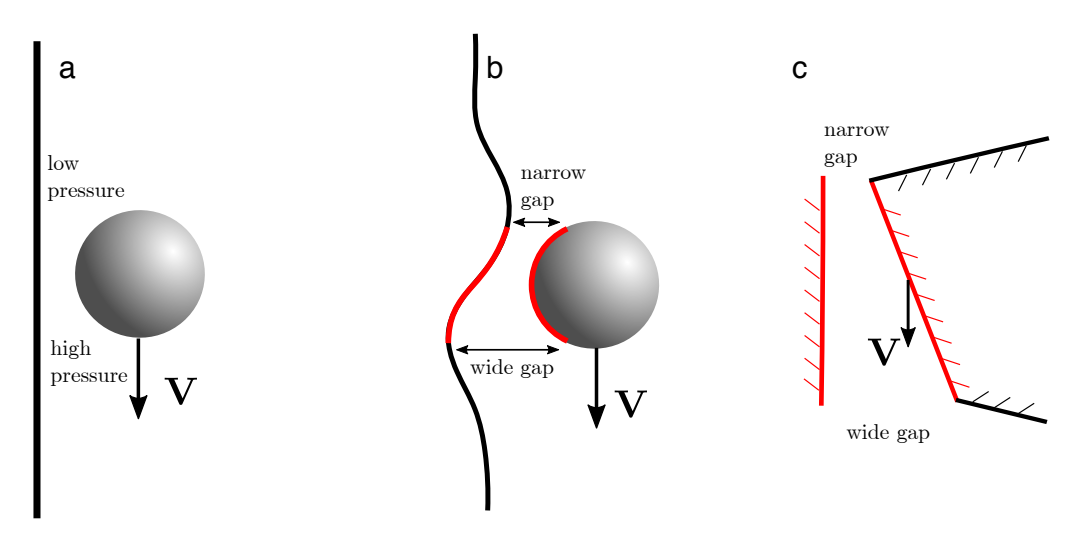


FIG. S2. The mechanism leading to the repulsive migration of the sphere: (a) In the zeroth-order problem, the sphere is translating next to a rigid wall. The generated pressure distribution is high in front of the sphere and low in the back. (b) Relaxing the rigidity constraint of the wall allows the generated pressure to deform the membrane. The antisymmetric deformation creates a wide gap in front of the sphere and a narrow gap at the back. This situation is analogous to (c) the problem of a flat-faced block moving parallel to a rigid wall [1], where the gap is wider in front of the block than at the back. Because the fluid flows from the wide to the narrow part of the gap (in the reference frame of the moving block), the generated pressure is higher on average than that outside the gap. Similarly, the next-order pressure in the hydroelastic surfing problem (b) is positive, resulting in a repulsive migration of the sphere.

C. Comparison with other elastic surfaces

Considering a few examples, we show that the repulsive forces generated by a membrane are a few orders of magnitude greater than those produced by a bulk elastic medium or an elastic coating on a rigid surface. We compare Eq. (7) of the Methods section with the results derived in [2]: for a cylinder moving next to a compressible elastic substrate, the force is

$$f_{\text{bulk}} \sim \frac{\mu^2 V_{\parallel}^2 a^2}{Gh^3},\tag{S1}$$

where G is the shear modulus of the material, while for similar motion near a soft coating of thickness δ ,

$$f_{\text{coating}} \sim \frac{\mu^2 V_{\parallel}^2 a^{3/2} \delta}{G h^{7/2}}.$$
 (S2)

Comparing a few cases:

1. A thin membrane (f_{membrane}), as we used in our experiments, relative to a thick bulk elastic surface of the same material (f_{bulk}), gives

$$\frac{f_{\text{membrane}}}{f_{\text{bulk}}} \sim \frac{\pi G(ah)^{3/2}}{B} \sim 10^3, \tag{S3}$$

where $G = \frac{E}{2(1+\nu)} = 83$ kPa is the shear modulus of the silicone rubber, and taking a = h = 5 mm, $B = 3.3 \,\mu\text{N}\cdot\text{m}$.

2. A thin membrane (f_{membrane}) compared with a soft coating on a rigid substrate (f_{coating}), such as the one used in [3] (G=65 kPa, elastic coating thickness $\delta=1.5$ mm, a=h=12.7 mm; a thin membrane of the same material of thickness b=0.25 mm has $B=2\mu\text{N·m}$), results in

$$\frac{f_{\text{membrane}}}{f_{\text{coating}}} \sim \frac{\pi G h^2 a^2}{B \delta} \sim 10^6.$$
 (S4)

3. A bacterium swimming next to a bio-membrane ($B \sim 10 \, k_B T$, $a \sim h \sim 10^{-6}$ m, $G \sim 100$ Pa) relative to motion next to a biological material such as the cytoskeleton, gives

$$\frac{f_{\text{membrane}}}{f_{\text{bulk}}} \sim 10^4. \tag{S5}$$

D. Effect of nonconstant tension along the sheet

Because the sheets are suspended under their own weight, the tension in the sheet is not constant but varies along the length of the sheet as

$$T(y) = \Delta \rho_s g b L \left(1 - \frac{y}{L} \right). \tag{S6}$$

In the main text, we approximate the tension by its mean $\frac{1}{2}\Delta\rho_s gbL$. Relaxing this approximation introduces two modifications. First, the restoring normal force on the membrane due to tension is proportional to $\nabla \cdot (T\nabla\zeta)$, which differs from $T\nabla^2\zeta$ (used in the main text) by a term of $O(\ell/L)$. This correction term is small since $\ell/L \leq 0.04$ in all of our experiments.

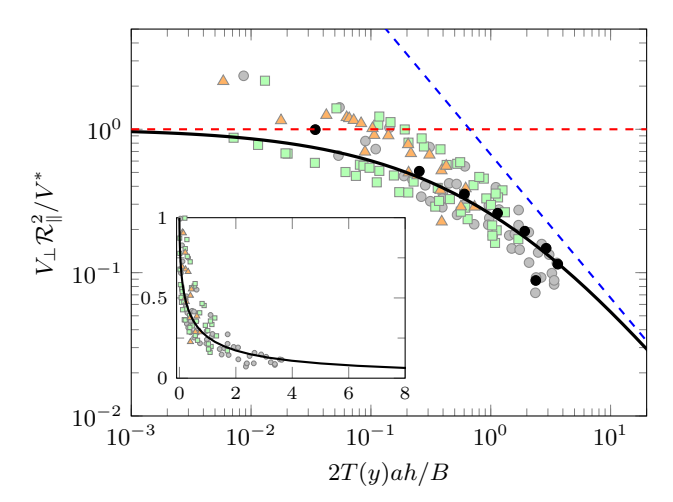


FIG. S3. Rescaled normal velocity $V_{\perp}\mathcal{R}_{\parallel}^2(H)/V^*$ versus the dimensionless tension $\tau H = 2T(y)ah/B$, where T(y) is given in Eq. (S6), showing the theoretical prediction (curves) and experimental data (symbols). Compare with Fig. 3 of the main text, where T(y) is approximated by its mean. Both figures contain identical data aside from the scaling of the abscissa.

Second, the varying tension along y modifies the relative importance of bending to tension along the trajectory of the particle. We show below that using Eq. (S6) for the tension instead of $\frac{1}{2}\Delta\rho_s gbL$ produces only small quantitative differences and does not affect the conclusions of the paper. Figure S3 replots the experimental data of Fig. 3 of the main text, but by scaling the horizontal axis with a dimensionless tension $\tau H = 2T(y)ah/B$, with both y(t) and h(t)

being instantaneously measured along the trajectory of the particle. The theoretical prediction (solid curve) is that of Eq. (3b) of the main text and remains unchanged. Comparing Fig. S3 below with Fig. 3 of the main text, it is clear that the qualitative behavior of the experimental data is not significantly influenced by the variation of tension along the sheet.

Figure S4 shows measured and computed trajectories of a particle taking into account the varying tension T(y) in the theory, providing a direct analog to Fig. 4 of the main text, which uses the mean tension in the trajectory computation. The results for h(t) and y(t) when both bending and tension are taken into account (black curve) are practically identical to their counterparts in Fig. 4 of the main text (constant tension).

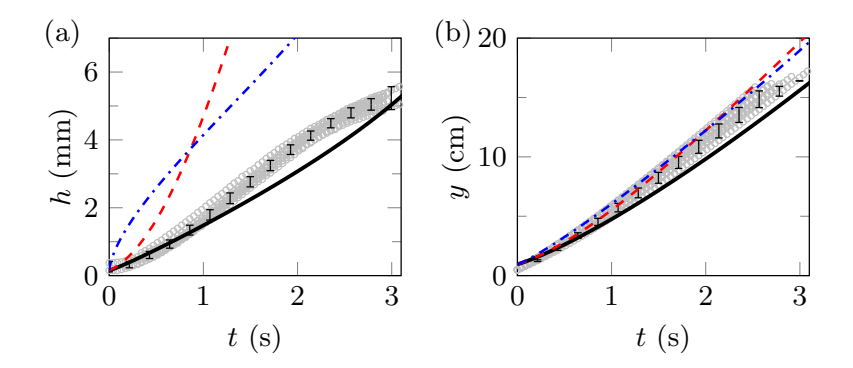


FIG. S4. Typical trajectories of a sphere showing experiments (symbols; error bars indicate one standard deviation) and theoretical predictions (curves) for varying tension T(y). Compare with Fig. 4 of the main text, where T(y) is approximated by its mean. The experimental data and parameters in both figures are identical.

E. Sedimentation near a rigid wall

Normal migration away from surfaces can also be produced due to the inertia of the flow. The Reynolds numbers in all of our experiments are small ($Re = \rho V_{\parallel} a/\mu \leq 0.25$). The inertial migration speed has been shown to scale as $ReV_{\parallel} f(h/a)$, where $f(h/a) \ll 1$ for $h/a \ll 1$ [4]. We verify the negligible role of inertia in our experiments by observing the sedimentation of spheres close to the rigid wall of the container in the absence of the sheets. We observe negligible normal migration of the sphere away from the rigid wall, in stark contrast to an experiment with identical parameters but with sedimentation near a freely suspended elastic sheet (Fig. S5). For the parameters in Fig. S5 (which correspond to the largest Reynolds number in our experiments), we infer from our measurements a normal migration speed away from the rigid wall (in the absence of the sheet) of $\lesssim 0.1$ mm/s, consistent with theoretical predictions of [4] for inertial migration.

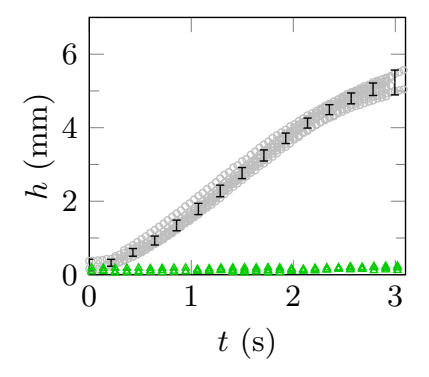


FIG. S5. Experimentally measured normal motion h(t) for a=5 mm glass spheres (Re=0.25) sedimenting near an elastic sheet with b=0.38 mm (circles; cf. Fig. 4 of main text and Fig. 4 above) and near the rigid container walls (triangles). Error bars indicate one standard deviation, with error bars for motion near the rigid wall (triangles) being within the size of the symbols. The results show that the normal migration is a direct consequence of the deformability of the sheet, and that inertial migration is negligible.

F. Active particles

Active particles propel without the action of an external driving force. Although this situation is in contrast with our experiments where motion is driven by gravity, we argue that active particles moving tangent to a flexible membrane experience a similar normal repulsive velocity due to hydroelastic coupling. First, we recognize that the flow around any particle can be expressed in terms of a Stokes multipole expansion (i.e. moments of the stress distribution on the particle's surface). In the case of an externally driven particle, the leading multipole corresponds to the force on the particle, which produces the fore-aft pressure asymmetry necessary to couple the tangential diving force to a normal repulsion via hydroelastic interactions. For an active particle, the leading singularity is a force dipole, which has the opposite symmetry of pressure and does not contribute to a normal force. Therefore, the next multipole in the expansion (the force quadrupole) is the dominant fore-aft pressure-asymmetric mode and will result in normal motion due to coupling. All odd force multipoles will result in normal hydroelastic migration due to tangential motion; for swimmers in close proximity to a membrane, higher terms in the expansion are not generally small.

G. Thermal fluctuations

In the absence of tension, thermal fluctuations could cause considerable height fluctuations. For red-blood cells $(a \sim 6-8 \mu \text{m})$, fluctuations of 0.3 μm in height were observed [5]. Still, relative to the size of a bacteria or a nearby particle, these may be small and we can consider the fluctuating membrane as an effective medium with a different bending rigidity. Previous work [6, 7] predicts that fluctuations reduce the bending rigidity of both fluid membranes and non-crystalline solid membranes [7]. For fluid membranes, Peliti and Leibler use renormalization group to show that the bending rigidity now depends on the length-scale of interest [6]:

$$B_{\text{eff}} = B + \frac{3k_B \mathcal{T}}{4\pi} \log(kr_m), \tag{S7}$$

where k is the wavenumber and r_m is a molecular length scale. Taking r = 5 Å, and $k = 2\pi/\ell$ with $\ell \sim 2 \mu m$ for a bacterium, gives $B \sim 8 \cdot 10^{-21}$ J, slightly reducing the bending rigidity, producing a greater migration velocity.

A second possible source of thermal noise is due to fluctuations of the particles themselves. The focus of our work is on objects that are either driven by external forces or are self-propelled. Examples in biological contexts at small scales include the motion of self-propelled (swimming) bacteria or spermatozoa near cell membranes, or the directed motion of molecular motors. In such cases the directional motion usually dominates over diffusion, i.e. large Peclét number $V_{\parallel}a/D\gg 1$ (for a bacterium $a\sim 2~\mu\text{m},~V_{\parallel}\sim 30~\mu\text{m/s}$ and $D\sim 0.1~\mu\text{m}^2/\text{s}$, the Péclet number is $\gtrsim 5000$). This directional motion of the object can then lead to a hydroelastic force as discussed in the main text. The influence of thermal fluctuations on these systems is expected to be subdominant.

We note that thermal fluctuations of the particle may also directly contribute to hydroelastic migration, in particular because V_{\perp} is quadratic in the forcing (in this case the thermal forcing). A more careful analysis of the coupled stochastic fluid-elastic problem that includes the dynamical response of the particle-membrane system is necessary to address this problem quantitatively.

^[1] Leal, L. G. Advanced Transport Phenomena: Fluid Mechanics and Convective Transport Processes (Cambridge University Press, 2007).

^[2] Skotheim, J. M. & Mahadevan, L. Soft lubrication. Phys. Rev. Lett. 92, 245509 (2004).

^[3] Saintyves, B., Jules, T., Salez, T. & Mahadevan, L. Self-sustained lift and low friction via soft lubrication. *Proc. Nat. Acad. Sci.* 113, 5847–5849 (2016).

^[4] Becker, L. E., McKinley, G. H. & Stone, H. A. Sedimentation of a sphere near a plane wall: weak non-Newtonian and inertial effects. *J. Non-Newt. Fluid Mech.* **63**, 201–233 (1996).

^[5] Brochard, F. & Lennon, J. Frequency spectrum of the flicker phenomenon in erythrocytes. J. de Phys. 36, 1035–1047 (1975).

^[6] Peliti, L. & Leibler, S. Effects of thermal fluctuations on systems with small surface tension. Phys. Rev. Lett. 54, 1690 (1985).

^[7] Nelson, D. & Peliti, L. Fluctuations in membranes with crystalline and hexatic order. J. de Phys. 48, 1085–1092 (1987).